View metadata, citation and similar papers at core.ac.uk
brought to you by CORE
provided by University of Queensland eSpace

TENSILE BEHAVIOUR OF FRP GRID STRENGTHENEING ECC COMPOSITE UNDER A UNIAXIAL LOADING

Yu-Zhou Zheng, Wen-Wei Wang *
Department of Bridge Engineering, School of Transportation, Southeast University.
No.2 Sipailou Road, Nanjing City, 210096, China. *Email: wangwenwei@seu.edu.cn

ABSTRACT

As the fibre reinforced polymer (FRP) sheets/textiles strengthening the inorganic cementitious materials technique was presented by some researchers, a few of potential shortcomings, such as penetrating difficultly of cementitious materials to and much brittle of FRP sheets, have been found in recent years. Therefore, a new strengthening system, which was FRP grid strengthening ECC system, in combination with the Engineered Cementitious Composites (ECC) and FRP grid was proposed by the present authors. By applying this system to reinforce the reinforced concrete (RC) beams, the dual strengthening effects can be provided and the intermediate crack-induced debonding failure can also be suppressed by externally bonded the FRP gird reinforced ECC composite layer to the tensile surface of the original RC beams. To investigate the tensile mechanical behaviour of FRP gird reinforced ECC composite layer, six non-strengthened ECC specimens and eighteen basalt fibre reinforced polymer grid (BFRP) strengthening ECC composite specimens (FRP-ECC specimens) subjected to the unidirectional axial tensile loading were conducted in this paper. Three kinds of different thickness BFRP grid were applied to investigate their reinforcement effects. The test results showed that there was no slip at the interface of BFRP grid and ECC substrate significantly. The failure modes were the internal PVA fibers ruptured or pulled out from ECC substrate for the non-strengthened ECC specimens and the rupture of BFRP reinforcements of grid for the strengthened FRP-ECC specimens. The axial stiffness of FRP-ECC specimens and the ultimate tensile stress and strain were obviously increased after the ECC substrate cracked, which indicated the contribution of the internal BFRP grid reinforcements. Moreover, an analytical model was also presented to predict the stress-strain relationship and the tensile strength of the FRP-ECC specimens and validated through comparison with the rest results.

KEYWORDS

Tensile behaviour, FRP Grid, Strengthening, ECC, Composite

INTRODUCTION

With the deepening of research works and wide applications of fiber reinforced polymer (FRP) composites in strengthening reinforced concrete (RC) elements, a few of potential drawbacks, such as interfacial debonding and poor resistance ability of epoxy resin for fire and ultraviolet (UV), have been realized by some scholars when using the epoxy resin as the bond and impregnated agents in recent years (Wang *et al*. 2012; Wang *et al*. 2013a; Wang *et al*. 2013b; Wang *et al*. 2014; Zhang *et al*. 2014). Therefore, the inorganic cementitious materials were applied to replace the epoxy resin so as to develop the relatively new strengthening techniques, e.g., the FRIP (fiber-reinforced inorganic polymer) (Dai *et al*. 2014; Ding *et al*. 2014), TRM (textile reinforced mortars) (Al-Salloum *et al*. 2012; D Ambrisi *et al*. 2012; Chalioris *et al*. 2014; Larrinaga *et al*. 2014; D'Ambrisi *et al*. 2015; Escrig *et al*. 2015) and cement based dry fiber sheets (Hashemi. S *et al* 2009; Zhang *et al*. 2014). Even so, the inorganic cementitious materials are much brittle and may be difficult to penetrate when fiber sheets/textiles are used as the reinforcing materials. For this purpose, an innovated strengthening system, FRP grid strengthening engineered cementitous composites (FRP-ECC strengthening system), in combination with the FRP grid and engineered cementitious composite (ECC) has been presented by the authors (Zheng *et al* 2015). In this system, FRP grid acts as the internal reinforcement and the ECC is applied as a bonding agent between the FRP grid and the concrete substrate. The authors hope the dual strengthening effects can be provided and the intermediate crack-induced debonding failure can also be suppressed by externally bonded the FRP gird reinforced ECC composite to the tensile surface of the original concrete RC beams.

Before implementing the FRP-ECC strengthening system, some basic research works should be conducted. One is most important to determine the stress-strain relationship (i.e. constitutive relation) of FRP gird strengthening ECC composite layer. Furthermore, the numerical simulations using the finite element analysis software and the analytical works for predicting the flexural and shear capacities of strengthened RC beams can be resolved after achieving the key constitutive relation of that composite material. Therefore, an experimental program was done to try to obtain the stress-strain relationship under the uniaxial loading, and an analytical model for predicting tensile capacity of FRP gird reinforced ECC composite was also presented based on the test results in this paper.

EXPERIMENTAL PROGRAMS

A total of twenty-four specimens subjected to the unidirectional loading were manufactured in this test program. Among them, six non-strengthened ECC specimens and eighteen FRP grid strengthening ECC (FRP-ECC) composite specimens were made to study their tensile mechanical performance. All test specimens were divided into four groups (i.e. Group E0, Group FE1, Group FE3 and Group FE5) and each group had six same specimens, as listed in Table 1. The ECC and FRP-ECC composite specimens were both the sheet shape and had the same geometrical dimension with 400 mm in length, 100 mm in width and 30 mm in thickness, as shown in Figure 1. The non-metallic reinforcement material embedded in the ECC substrate was basalt fiber reinforced polymer (BFRP) grid. The dimension of BFRP grid were 100 mm in width and 400 mm in length and the orthogonal BFRP reinforcements were arranged at a space of 50 mm center to center along the longitudinal and transverse directions, as indicated in Figure 2. To investigate the effect of internal reinforcement, three kinds of different thickness (i.e. 1 mm, 3 mm and 5 mm) BFRP grids were used in this test program. Moreover, two 100 mm ×100 mm thin square aluminium plates were attached to the cement-base surface at the two ends of specimens to ensure those specimens can be clamped tightly with the stretching machine, as shown in Figure 1. The details of all test specimens are summarised in Table 1.

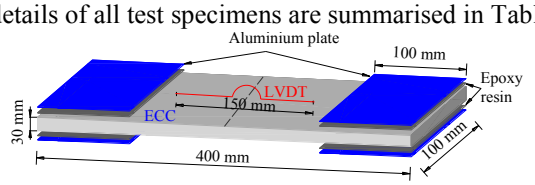

Figure 1 FRP-ECC specimen

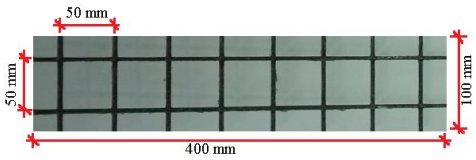

Figure 2 BFRP grid coupon

Before the unidirectional tensile test, nine BFRP grid coupons (i.e. three coupons for 1 mm, 3 mm and 5 mm, respectively) were prepared to determine their mechanical behavior. The geometrical dimension of BFRP grid coupons were the same with that of the BFRP grids used for strengthening FRP-ECC composite specimen. The average tensile strengths of 1 mm, 3 mm and 5 mm thick BFRP grids were 357 MPa, 386 MPa and 416 MPa, respectively, while the average elastic module were 51 GPa, 53 GPa and 57 GPa, respectively. As a result, the average elongation was 27%, 26% and 22%, respectively. ECC was made from the ordinary Portland cement, fly ash, fine sand, polyvinyl alcohol (PVA) fiber and some admixtures. The Polyvinyl Alcohol (PVA) fibre used for making ECC was produced by a Japanese company. All material properties of PVA fibres were listed in Table 1 and the mixed proportion of ECC were designed in the Table 2.

Table 1 Material properties of PVA fibres

Diameter (μm)	Length (mm)	Density (g/cm^3)	Elastic module (GPa)	Tensile strength (MPa)	Elongation (%)
39	12	1.3	40	1530	7

Table 2 Mixed proportion of ECC

Water (kg)	Cement (kg)	Fly ash (kg)	Silica sand (kg)	Fiber volume content (%)	Silica fume (kg)	Water reducer (kg)	Water/cement materials (%)
0.33	0.40	1.00	0.32	2	0.040	0.005	46

After all specimens were cured 28-day in a curing chamber with a temperature of 20 centigrade degree and a relative humidity of 95%, the unidirectional tensile test was conducted. The specimens were placed into and then clamped by two steel collets of the computer-controlled universal testing machine, as shown in Figure 3. One 'Ω' shape linear variable displacement transducers (LVDT) was bonded to one side surface of the tested specimen to measure the longitudinal deformation and the initial measuring distance (i.e. the gauge length) was 150 mm, as seen in Figure 3. The loading was run by the displacement and the implementary rate was 0.5 mm/min uniformly in the whole test process. The applied loading and the longitudinal deformation were both acquired by an automatic acquisition system.

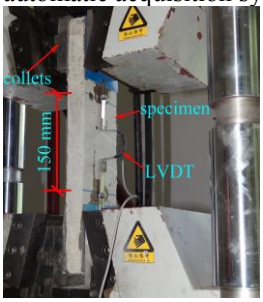

Figure 3 Details of test setups

(a) ECC specimen

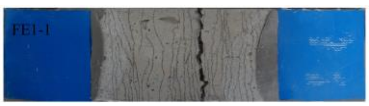

(b) FRP-ECC composite specimen

Figure 4 Failure modes

Table 3 Details of specimens and summary of test results

ID	Type of specimen	Thickness of BFRP Grid (mm)	Cracking stage				Ultimate stage				correction coefficient α	Predicting model			
			Stress $\sigma_{fe,cr}$ (MPa)	Strain $\varepsilon_{fe,cr}$ ($\mu\varepsilon$)	Load $P_{cr,t}$(kN)	Tangent slopes E_1	Stress $\sigma_{cu,t}$ (MPa)	Strain $\varepsilon_{cu,t}$ ($\mu\varepsilon$)	Load $P_{cr,t}$(kN)	Tangent slopes E_2		Cracking load $P_{cr,p}$ (kN)	$P_{cr,t}/P_{cr,p}$	Ultimate load $P_{u,p}$ (kN)	$P_{u,t}/P_{u,p}$
E0-1	ECC	None	2.50	368	7.50		2.84	11360	8.52						
E0-2			2.52	421	7.56		2.84	10106	8.52						
E0-3			2.05	304	6.15		2.76	9135	8.28						
E0-4			2.80	395	8.40		3.00	9264	9.00						
E0-5			1.57	295	4.71		2.23	8655	6.69						
E0-6			2.19	353	6.57		2.53	10048	7.59						
FE1-1	FRP-ECC	1	2.90	366	8.70	7931	3.89	10155	11.67	101	0.65	8.70	1.18	11.24	1.04
FE1-2			2.80	309	8.40	9061	3.85	12048	11.55	115	0.74	8.40	1.14	11.24	1.03
FE1-3			3.00	314	9.00	9554	4.20	10837	12.60	114	0.65	9.00	1.22	11.24	1.12
FE1-4			2.49	372	7.47	6694	4.03	11393	12.09	140	0.67	7.47	1.09	10.70	1.13
FE1-5			2.62	320	7.86	8188	4.05	11454	12.15	128	0.52	7.86	1.15	10.70	1.13
FE1-6			2.53	363	7.59	6970	4.04	13275	12.12	117	0.70	7.59	1.11	10.70	1.13
FE3-1		3	3.01	390	9.03	7718	5.61	11343	16.83	237	0.62	9.03	1.20	15.82	1.06
FE3-2			2.54	399	7.62	6366	6.04	15258	18.12	236	0.51	7.62	1.01	15.82	1.15
FE3-3			2.36	365	7.08	6466	5.77	16900	17.31	206	0.52	7.08	0.94	15.82	1.09
FE3-4			2.00	421	6.00	4751	5.40	17819	16.20	195	0.46	6.00	0.85	15.29	1.06
FE3-5			2.72	411	8.16	6618	5.65	15864	16.95	190	0.65	8.16	1.16	15.29	1.11
FE3-6			2.32	411	6.96	5645	5.42	12843	16.26	249	0.55	6.96	0.99	15.29	1.06
FE5-1		5	2.51	365	7.53	6877	7.03	17619	21.09	262	0.50	7.53	0.97	20.47	1.03
FE5-2			3.07	344	9.21	8924	6.35	12663	19.05	266	0.65	9.21	1.19	20.47	0.93
FE5-3			3.13	373	9.39	8391	7.95	16795	23.85	294	0.61	9.39	1.22	20.47	1.16
FE5-4			2.25	324	6.75	6944	7.07	14910	21.21	330	0.51	6.75	0.93	19.96	1.06
FE5-5			2.95	378	8.85	7804	8.13	17237	24.39	307	0.57	8.85	1.22	19.96	1.22
FE5-6			2.67	425	8.01	6282	7.80	13882	23.40	381	0.46	8.01	1.10	19.96	1.17
	Average value										0.57		1.09		1.09
	Standard deviation												0.11		0.06
	COV												0.10		0.06

RESULTS AND DISCUSSIONS

Failure modes

Two failure modes were observed in those specimens. For the non-strengthened ECC specimens (i.e. Group E0), the internal PVA fibers were fractured or pulled out from the cement base at a certain section, as shown in Figure 4(a). For the BFRP grid strengthening ECC (FRP-ECC) specimens, the rupture of one longitudinal reinforcements of the BFRP grid was observed at the location of maximum crack width, as shown in Figure 4(b).

Specimens in Group E0 were used as the reference specimens without the reinforcement material of BFRP grid. The first fine crack was formed at the middle section of the specimen shortly after the external loading applied. Then more fine cracks were appeared uniformly along the longitudinal direction of specimen and propagated toward two side edges of specimen as the applied loading increased. When the ultimate load applied, the specimen were eventually separated two parts along a main crack, which indicated the final failure occurred. For the specimens were internally strengthened with 1 mm thickness of BFRP grid (i.e. Group FE1), a few of fine cracks were observed on the surface of specimen when the load approached to 8.20 kN (average measured value of six specimens) or approximately 68% of ultimate load. With the load further increased, some new fine cracks were constantly formed and old fine cracks extended to the both sides of specimen. When the load was applied to the 12.03 kN (average measured value of six specimens), slightly "cracking" sound from the BFRP grid was heard and one longitudinal reinforcement of BFRP grid was finally ruptured at the position of main crack. For all the rest of strengthened specimens (Groups FE-3 and FE-5), the similar tensile behavior were observed during the whole testing process.

Stress-strain responses

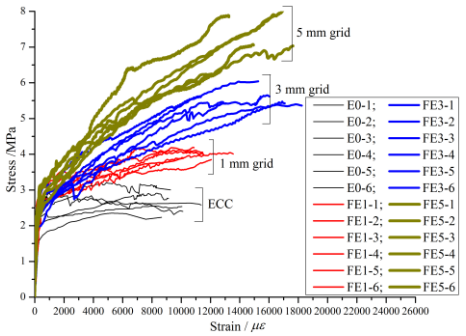

Figure 5 Stress-strain curves of all tested specimens

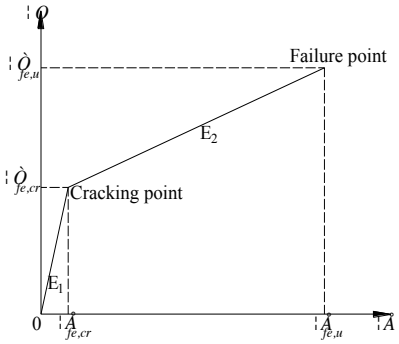

Figure 6 Proposed stress-strain relationship model

Figure 5 presents the stress-strain response of all tested specimens under the uniaxial tensile loading. It should be noted that the tensile stress shown in Figure 5 can be obtained as:

$$\sigma_{fe} = P_t / A_{fe} \quad (1)$$

Where σ_{fe} is the tensile stress of the test specimen; P_t is the applied loading and A_{fe} is the cross-sectional area of the test specimen neglecting the cross-sectional area of BFRP grid. The corresponding strain can be deduced as:

$$\varepsilon_{fe} = \Delta L / L \quad (2)$$

Where ε_{fe} is the tensile strain of the test specimen; ΔL is the increment of gauge length and L is the gauge length (i.e. 150 mm).

It is apparently observed from Figure 5 that the stress-strain curves for the non-strengthened ECC and FRP-ECC specimens can be divided into two stages. In the first stage, the strain is a linear growth with the stress increasing before ECC cracked. Therefore, this stage can be considered to be the linear-elastic stage. After ECC cracked, the growth rate of strain is greater than that of stress and the slope of stress-strain curves is changed due to the axial stiffness decreased continuously. For the ECC specimens, lager strain is observed while the stress almost is kept a constant value in the second stage (see the stress-strain curves of ECC in Figure 5). This phenomenon is well known as the strain-hardening performance of ECC. For the specimens strengthened with different thickness BFRP grid, the axial stiffness remains increasement due to the contribution of the internal BFRP reinforcements. Moreover, the combined action of ECC and BFRP grid results in a larger ultimate tensile strain compared with ECC specimen. Here we define the stress corresponding to the crack loading of specimen as the cracking stress. Therefore, the corresponding axial tensile strain is defined as the cracking strain. The key

values of stress and strain for each specimen at the different stages (i.e. crack and ultimate stages) are listed in Table 1.

It is found from Table 1 that the average cracking stress increases from 2.28 MPa for the ECC specimen to 2.73 MPa, 2.50 MPa and 2.76 MPa for the strengthened FRP-ECC specimens in Group FE1, Group FE3 and Group FE5 respectively, which indicates the effective tensile contribution of BFRP grid for the ECC cementitious base. Furthermore, there is a remarkable improvement in the ultimate stress when the internal BFRP grid was added. The increase of ultimate stress ranges from 49% to 174% for the strengthened FRP-ECC specimens compared to the non-strengthened reference specimens.

PREDICTED MODEL

As seen from the above tensile test results, the stress-strain response of FRP-ECC specimens can be divided into two stages. Therefore, a bi-linear theoretical model based on the test results is presented in this section to define the stress-strain relationship of the FEP-ECC composite under the uniaxial loading, which is:

$$\sigma_{fe} = \begin{cases} E_1 \varepsilon_{fe} & (0 \le \varepsilon_{fe} \le \varepsilon_{fe,cr}) \\ E_2(\varepsilon_{fe} - \varepsilon_{fe,cr}) + \sigma_{fe,cr} & (\varepsilon_{fe,cr} \le \varepsilon_{fe} \le \varepsilon_{fe,u}) \end{cases} \tag{3}$$

Where E_1, E_2 is the tangent slopes of stress-strain curve for the FRP-ECC composite at the first and second stages, respectively; $\varepsilon_{fe,cr}$ and $\varepsilon_{fe,u}$ is the cracking strain and ultimate strain of FRP-ECC composites, respectively. $\sigma_{fe,cr}$ is the cracking stress of FRP-ECC composite corresponding to the cracking strain $\varepsilon_{fe,cr}$.

To determine the stress-strain relationship of the FRP-ECC composite, the values of E_1, E_2, $\varepsilon_{fe,cr}$ and $\varepsilon_{fe,cu}$ should be obtained firstly. As shown in Figure 6, a non-cracked FRP-ECC composite specimen is consisted of the ECC cementitious base and internal BFRP grid. Based on the equilibrium conditions of the axial forces acted on the each material element, the following equation can be deduced:

$$E_{fe}\varepsilon_{fe}A_{fe} = E_e\varepsilon_e A_e + E_f\varepsilon_f A_f \tag{4}$$

Where E_{fe} ,E_e and E_f is the elastic modulus of FRP-ECC composite, ECC layer and BFRP grid, respectively ; ε_e and ε_f is the tensile strain of ECC and BFRP grid, respectively; A_{fe}, A_e and A_f is the cross section area of FRP-ECC composite, ECC layer and BFRP grid, respectively .

If considering $\varepsilon_{fe} = \varepsilon_e = \varepsilon_f$, Equation (4) can be rewritten as:

$$E_{fe} = E_e + E_f \frac{A_f}{A_{fe}} \tag{5}$$

In fact, the elastic modulus of FRP-ECC composite could be decreased due to the stress softening and the development and formation of the internal micro-crack of ECC cementitious base (Contamine *et al*. 2011; Contamine *et al*. 2014). Therefore, a reduction coefficient α is induced to reflect the influences of those factors and Equation (5) can be given as:

$$E_1 = \alpha E_{fe} = \alpha\left(E_e + E_f \frac{A_f}{A_{fe}}\right) \tag{6}$$

Where E_1 is the modified elastic modulus of FRP-ECC composite and can be thought of as the tangent slope of the stress-strain curve at the first stage. Substituting the measured values of the tangent slope of the stress-strain curve at the first stage and the relative values of the elastic modulus and the cross-section area of the ECC and BFRP grid into Equation (6), the reduction coefficient α can be obtained as list in Table 1.Taking the average value of the reduction coefficient α for all FRP-ECC composite specimens, we can obtain:

$$\alpha = 0.57 \tag{7}$$

The tangent slope E_2 of stress-strain curve at second stage is mainly affected by the elastic modulus of FRP grid after ECC cracked. Therefore, the second stage tangent slope E_2 can be obtained through regressing the measured values of E_2 and the elastic modulus of FRP grid E_f (Figure 8):

$$E_2 = 0.03E_f - 1468 \tag{8}$$

As discussed above, the cracking load of FRP-ECC was primarily determined by the tensile strength of the ECC cementitious base. Thus, it is assumed the cracking strain of FRP-ECC composite is equal to that of ECC, and taken as $\varepsilon_{fe,cr} = \varepsilon_{e,cr}$ (where $\varepsilon_{e,cr}$ is the cracking strain of ECC cementitious base). Whereas, the ultimate strain of FRP-ECC composite mainly depended on the ultimate strain of BFRP grid. After analyzing the measured ultimate strain of FRP-ECC composite carefully, it can be found that there is no regular relation between ultimate strain of FRP-ECC composite and the ultimate strain of BFRP grid. Hence, an empirical coefficient γ is introduced and the following equation is given:

$$\varepsilon_{fe,u} = \gamma\varepsilon_{fu} \tag{9}$$

In which, $\varepsilon_{fe,u}$ and ε_{fu} is the ultimate strain of FRP-ECC composite and BFRP grid, respectively. By averaging the ratios of the measured ultimate strain of FRP-ECC composite specimens and that of BFRP grid (i.e. $\gamma = \varepsilon_{fe,u} / \varepsilon_{fu}$), the value of empirical coefficient γ is equal to:

$$\gamma = 1.97 \tag{10}$$

After determining stress-strain relationship of FRP-ECC composite, the predicted cracking load $P_{cr,p}$ and ultimate load $P_{u,p}$ can be respectively given as:

$$\begin{cases} P_{cr,p} = \sigma_{fe,cr} A_{fe} \\ P_{u,p} = \sigma_{fe,u} A_{fe} \end{cases} \tag{11}$$

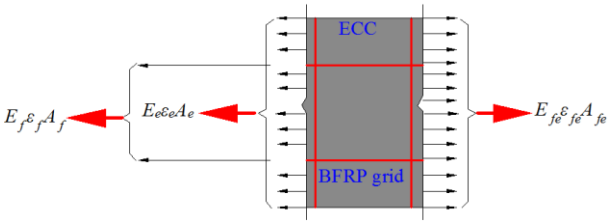

Figure 7 Analytical model

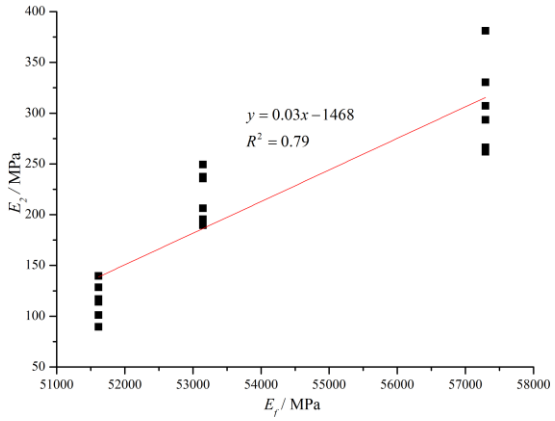

Figure 8 Regression of tangent slope E_2

Two FRP-ECC composite specimens FE3-3 and FE5-4 were selected to validate the accuracy of the analytical model. The experimental and predicated stress-strain curves were shown in Figure 9. Moreover, the predicated values of the cracking and ultimate loads for all strengthened specimens were list in Table1. It should be noted that the predicted curves follows very closely to the experimental one with the slightly discrepancies. Furthermore, the average ratio of experimental values to the predicated ones is 1.09 for both the cracking load and the ultimate load and the coefficient of variation (COV) is 0.10 for the cracking load, 0.06 for the ultimate load, respectively. Therefore, the reliability of proposed model for predicting the stress-strain relationship and the tensile strength of the FRP-ECC composite under the unidirectional loading is validated.

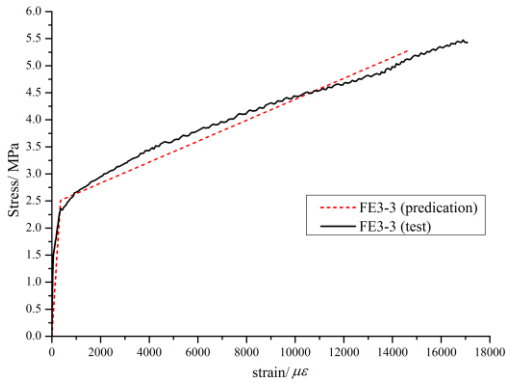

(a) Specimen FE3-3

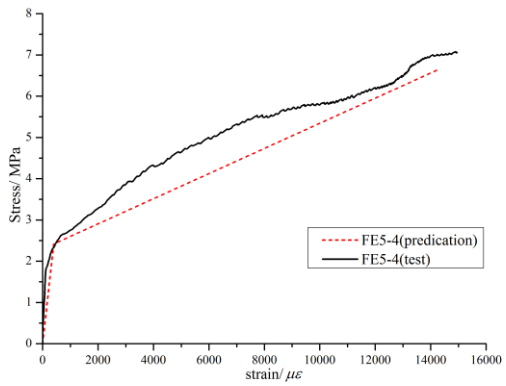

(b) Specimen FE5-4

Figure 9 Comparisons between the experimental stress-strain curves and predicated one of specimens FE3-3 and FE5-4

CONCLUSIONS

(1) The final failure modes of the internal PVA fibers ruptured and then pulled out from ECC for the control non-strengthened specimen and the rupture of BFRP reinforcements for the FRP-ECC composite specimen were observed in the test program.

(2) After strengthened with BFRP grid, the axial stiffness, the ultimate tensile stain and the tensile strength of the FRP-ECC specimens were greatly improved compared with the non-strengthened specimens, which showed the effective contribution of the internal FRP grid for improving the tensile performance of the strengthen FRP-ECC composite.
(3) An analysis method has been proposed for predicting the material constitutive relation and the tensile capacity of FRP-ECC composite and its validity is demonstrated through comparisons with test results.

ACKNOWLEDGMENTS

The authors would like to express their acknowledgments to the National Natural Science Foundation of China (Programs No. 51278441 and 51578135) and Graduate Scientific Research and Innovation Projects in Jiangsu province（Program No. KYLX15_0142）for providing the supporting funds for this research work.

REFERENCES:

Al-Salloum, Y. A., Elsanadedy, H. M., Alsayed, S. H., and Iqbal, R. A. (2012). "Experimental and numerical study for the shear strengthening of reinforced concrete beams using textile-reinforced mortar." *Journal of Composites for Construction*, 16(1), 74-90.

Chalioris, C. E., Thermou, G. E., and Pantazopoulou, S. J. (2014). "Behaviour of rehabilitated RC beams with self-compacting concrete jacketing-Analytical model and test results." *Construction and Building Materials*, 55, 257-273.

D Ambrisi, A., Feo, L., and Focacci, F. (2012). "Bond-slip relations for PBO-FRCM materials externally bonded to concrete." *Composites Part B: Engineering*, 43(8), 2938-2949.

Dai, J., Munir, S., and Ding, Z. (2014). "Comparative study of different cement-based inorganic pastes towards the development of FRIP strengthening technology." *Journal of Composites for Construction*, 18, (A40130113SI), 1-10.

Contamine, R., Junes, A., and Si Larbi, A. (2014). "Tensile and in-plane shear behaviour of textile reinforced concrete: Analysis of a new multiscale reinforcement." *Construction and Building Materials*, 51, 405-413.

Contamine, R., Si Larbi, A., and Hamelin, P. (2011). "Contribution to direct tensile testing of textile reinforced concrete (TRC) composites." *Materials Science and Engineering: A*, 528(29-30), 8589-8598.

D'Ambrisi, A., Focacci, F., Luciano, R., Alecci, V., and De Stefano, M. (2015). "Carbon-FRCM materials for structural upgrade of masonry arch road bridges." *Composites Part B: Engineering*, 75, 355-366.

Ding, Z., Dai, J., and Muner, S. (2014). "Study on an improved phosphate cement binder for the development of fiber-reinforced inorganic polymer composites." *Polymers*, 6(11), 2819-2831.

Escrig, C., Gil, L., Bernat-Maso, E., and Puigvert, F. (2015). "Experimental and analytical study of reinforced concrete beams shear strengthened with different types of textile-reinforced mortar." *Construction and Building Materials*, 83, 248-260.

Hashemi. S, and Al-mahaidi, R. (2009). "Cement based bonding material for FRP strengthening of concrete structures." *Proceedings of the 9th international symposium on fiber-reinforced polymer reinforcement for concrete structures*, FRPRCS-9, 13-15 July, Sydney, Australia.

Larrinaga, P., Chastre, C., Biscaia, H. C., and San-José, J. T. (2014). "Experimental and numerical modeling of basalt textile reinforced mortar behavior under uniaxial tensile stress." *Materials & Design*, 55, 66-74.

Wang, W., Dai, J., Harries, K. A., and Bao, Q. (2012). "Prestress losses and flexural behavior of reinforced concrete beams strengthened with posttensioned CFRP sheets." *Journal of Composites for Construction*, 16(2), 207-216.

Wang, W., Dai, J., Harries, K. A., and Zhang, L. (2014). "Prediction of prestress losses in RC beams externally strengthened with prestressed CFRP sheets/plates." *Journal of Reinforced Plastics and Composites*, 33(8), 699-713.

Wang, W., Dai, J., and Harries, K. A. (2013a). "Intermediate crack-induced debonding in RC beams externally strengthened with prestressed FRP laminates." *Journal of Reinforced Plastics and Composites*, 32(23), 1842-1857.

Wang, W., Dai, J., and Harries, K. A. (2013b). "Performance evaluation of RC beams strengthened with an externally bonded FRP system under simulated vehicle loads." *Journal of Bridge Engineering*, 18(1), 76-82.

Zhang, L., Wang, W., Harries, K. A., and Tian, J. (2014). "Bonding behavior of wet-bonded GFRP-Concrete interface." *Journal of Composites for Construction*, (04015001), 1-14.

Zheng, Y., and Wang, W. (2015). "Flexural behaviour of reinforced concrete beams strengthened with a composite reinforcement layer: BFRP Grid and ECC." *Construction and Building Materials* (under review).